International Journal of Modern Physics A

Differential measurements of jet sub-structure observables and their correlations in $p{+}p$ collisions at $\sqrt{s} = 200$ GeV in STAR

Monika Robotková for the STAR Collaboration

Nuclear Physics Institute of the CAS, Husinec - Řež, 130 Řež, 250 68, Czech Republic

robotmon@fjfi.cvut.cz

January 30, 2022

Jets are collimated sprays of hadrons created by the fragmentation of high energy partons, and can serve as an experimental tool for studying quantum chromodynamics. In particular, we can explore the properties of parton shower and evolution by measuring jet sub-structure. One of the techniques that allows experimental access to the parton shower is the jet grooming technique called SoftDrop. This analysis extends recent measurements of the jet sub-structure observables based on the SoftDrop algorithm, including groomed radius (R_g) and shared momentum fraction (z_g), in p+p collisions at $\sqrt{s} = 200$ GeV in the STAR experiment. We present fully corrected multi-differential measurements of jet sub-structure observables at the first split and their correlations for jets of different transverse momenta and radii. To further explore the jet sub-structure, we present the first measurement of the jet sub-structure observables at the first, second and third splits via the iterative SoftDrop procedure. We show a strong dependence of the z_g on the R_g and the split number with the observation that selecting on narrower opening angles is similar to progressing further along the jet clustering tree. We compare our measurements to the state-of-the-art Monte Carlo models.

Keywords: Jet, sub-structure, SoftDrop.

1. Introduction

Jets are collimated sprays of hadrons reconstructed by clustering algorithms, and are created in collisions of high energy particles. Jet sub-structure allows us to explore the properties of Quantum ChromoDynamics (QCD) and parton shower experimentally. In our analysis we use a grooming technique called SoftDrop [1]. This technique is based on removing soft wide-angle radiation within a jet and connects the parton shower to an angular ordered clustering tree. In the SoftDrop procedure, jets are first reconstructed with the anti-k_T algorithm, which starts by clustering particles with the highest transverse momentum (p_T). Then jets are reclustered with the C/A algorithm [2] to obtain an angular ordered tree. By undoing the last step of the reclustering, each jet is divided into sub-jets labeled as 1 and 2. A jet is considered as a final SoftDrop jet if its sub-jets pass the condition,

$$\frac{\min(p_{T,1}, p_{T,2})}{p_{T,1} + p_{T,2}} > z_{cut} \left(\frac{\Delta R_{1,2}}{R} \right)^{\beta}, \tag{1}$$

where $p_{T,i}$ corresponds to the transverse momentum of the sub-jet, $\Delta R_{1,2}$ is the distance between the sub-jets, and R is the jet resolution parameter. If the sub-jets do not pass the condition, the one with higher p_T is denoted as the starting jet and the whole process is repeated. We set the SoftDrop parameters to $\beta = 0$ and $z_{cut} = 0.1$. The products of the SoftDrop procedure are shared momentum fraction (z_g) and groomed radius (R_g). Shared momentum fraction is defined as $z_g = \frac{\min(p_{T,1}, p_{T,2})}{p_{T,1}+p_{T,2}}$ and R_g is the first $\Delta R_{1,2}$ which satisfies the SoftDrop condition. We present the first use of iterative SoftDrop, a special condition of recursive SoftDrop [3], which follows splitting along the harder branch to study the evolution of the splitting kinematics along the jet shower.

Our goal is to study the parton showers experimentally through observables z_g and R_g. There are two options how to explore these observables: we can focus only on the first split and study the correlation between z_g and R_g as a function of jet p_T, or move along the jet shower and study the z_g and R_g distributions at the first, second and third splits.

2. Data analysis

Data were collected by the STAR experiment [4] located at the Relativistic Heavy Ion Collider at Brookhaven National Laboratory in 2012 for p+p collisions at $\sqrt{s} = 200$ GeV. For the analysis, only events selected by the Barrel Electromagnetic Calorimeter (BEMC) Jet Patch 2 (JP2) trigger, with a transverse energy threshold of $E_T > 7.3$ GeV, are used. Jets consist of charged particle tracks from the Time Projection Chamber (TPC) and neutral energy towers from the BEMC. We use only tracks from the TPC in the range of $0.2 < p_T < 30$ GeV/c, and BEMC towers with energy in the range of $0.2 < E_T < 30$ GeV. In order to avoid double counting of charged-track energies in the BEMC towers, hadronic correction [5] is applied.

Jets are reconstructed using the anti-k_T algorithm for resolution parameters $R = 0.4$ and $R = 0.6$. Jets are required to have $p_{T,jet} > 10$ GeV/c and to lie within the pseudorapidity $|\eta_{jet}| < 1.0 - R$.

3. Correlation between sub-structure observables at the first split

The jet sub-structure observables were previously measured by the ALICE [6], ATLAS [7], CMS [8] and STAR [9] experiments. The momentum and angular scales quantified by z_g and R_g observables have been so far measured separately by the STAR experiment [5]. Our goal is to extend this measurement and study the correlation between these two observables.

3.1. *2+1D unfolding*

Since measurements are always affected by the finite efficiency and resolution of the instrumentation, unfolding is needed to correct the detector effects. In our case, where the observables lie in a 3-dimensional ($p_{T,jet}$, z_g, R_g) space, we need to apply a multi-dimensional unfolding. We use the Iterative Bayesian unfolding to correct the 2D correlation between z_g and R_g, where a response matrix is estimated by matching particle-level spectra from PYTHIA 6 [10] with the STAR Perugia tune [11] to detector-level spectra obtained by passing PYTHIA 6 events through the GEANT3 simulator [12]. Unfolding is done separately for (z_g, R_g) correlation in four different detector-level $p_{\mathrm{T,jet}}$ intervals, namely $p_{\mathrm{T,jet}}^{\mathrm{det}} \in [15,20], [20,25], [25,30]$, and $[30,40]$ GeV/c. Lastly, the correction for $p_{\mathrm{T,jet}}$ scale and resolution is applied via selections on the response matrix (Fig. 1 of ref. [5]). The projections to the detector-level $p_{\mathrm{T,jet}}$ for particle-level $p_{\mathrm{T,jet}}$ bins are normalized to unity and used as weights for summing unfolded (z_g, R_g) correlations in different $p_{\mathrm{T,jet}}^{\mathrm{det}}$ bins. Additional corrections for trigger and jet finding efficiencies are applied and fully corrected results are presented for selected particle-level $p_{\mathrm{T,jet}}$ bins.

3.2. *Systematic uncertainties*

Systematic uncertainties arising from detector effects are estimated by adjusting the response matrix for unfolding, i.e. 4% in the TPC tracking efficiency and 3.8% in the BEMC tower calibration [5], and comparing with the normal values. For the hadronic correction uncertainty, we vary the fraction of track momentum subtracted from the matched BEMC tower from the nominal value of 100% to 50%. In the estimation of uncertainty coming from unfolding, the iterative parameter is changed from the nominal value of 4 to 6. Uncertainty due to the prior shape variation has not been estimated yet, and will be included in the final publication. An example of systematic uncertainties for z_g distributions in three R_g intervals for jets with $R = 0.4$ and $20 < p_{\mathrm{T,jet}} < 25$ GeV/c is shown in Fig. 1. The total uncertainty ranges between 5 and 10% and the largest contributions come from the hadronic correction and unfolding.

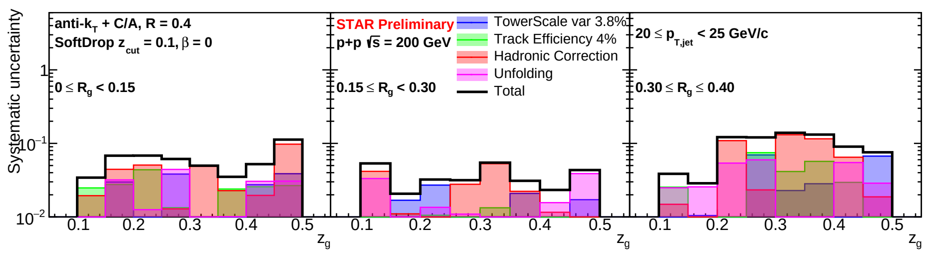

Fig. 1. Systematic uncertainties for z_g in three R_g bins for jets with $R = 0.4$ and $20 < p_{\mathrm{T,jet}} < 25$ GeV/c in p+p collisions at $\sqrt{s} = 200$ GeV.

3.3. *Results and comparison with Monte Carlo models*

Fully unfolded z_g distributions at the first split for different R_g and $p_{\mathrm{T,jet}}$ bins are shown in Fig. 2. Three R_g bins are plotted with different colors, where blue, red and black correspond to $0 \le R_g < 0.15$, $0.15 \le R_g < 0.30$ and $0.30 \le R_g \le 0.40$, respectively. Bands around the data points indicate the systematic uncertainties described in Sec. 3.2.

We observe that the z_g distribution gradually changes its shape to be steeper for larger R_g, implying softer splits. This also indicates that jets with a smaller first split R_g have an increased probability of harder collinear splits. The distributions change only mildly with increasing $p_{T,jet}$, which means that R_g is the driving factor in determining the shape of the z_g distribution.

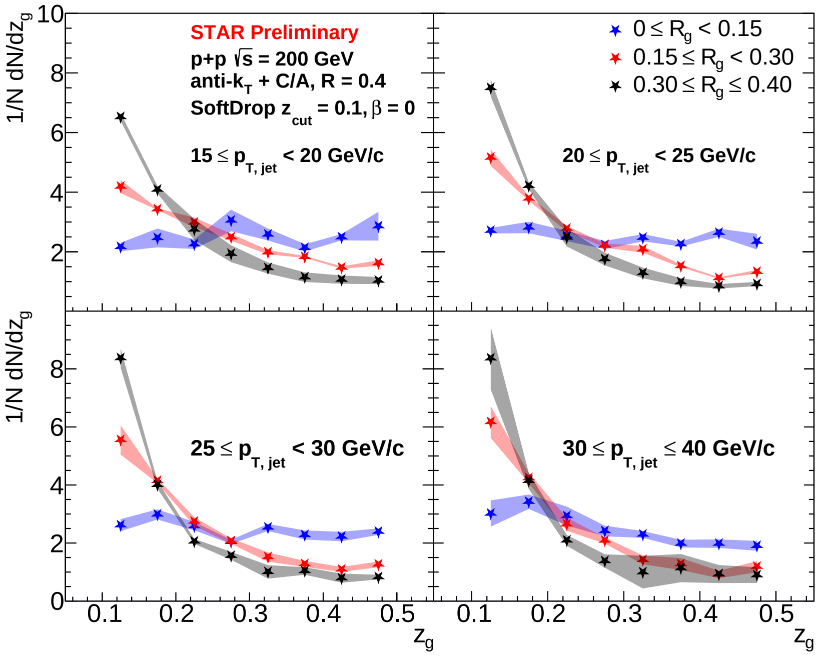

Fig. 2. Fully unfolded z_g distributions for three R_g bins for jets with $R = 0.4$ in p+p collisions at $\sqrt{s} = 200$ GeV. Individual panels correspond to different $p_{T,jet}$ intervals (see legend).

The corrected z_g distributions for different R_g are compared to predictions from several Monte Carlo (MC) generators, as shown in Fig. 3. We use PYTHIA 6 with the STAR Perugia tune, PYTHIA 8 [13] with the Monash tune based on LHC data [14], and HERWIG 7 [15] with the EE5C tune [16]. These models have different implementations of parton shower and hadronization. Parton shower in HERWIG is angularly ordered in contrast to both PYTHIA versions, where the k_T or p_T ordering is used. For the hadronization, the cluster model and the Lund string model are used in HERWIG and PYTHIA, respectively. We observe that all MC models describe the trend of the data, but there are slight differences across the varying R_g bins which will be studied in detail in an upcoming publication.

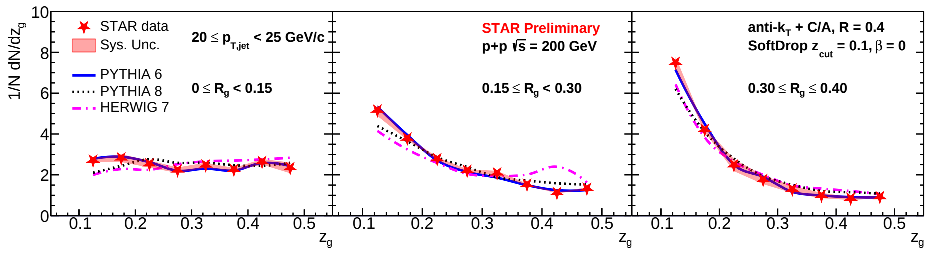

Fig. 3. Fully unfolded z_g distributions in three R_g bins for jets with $R = 0.4$ and $20 < p_{T,jet} < 25$ GeV/c in p+p collisions at $\sqrt{s} = 200$ GeV, compared with Monte Carlo simulations from PYTHIA 6, PYTHIA 8 and HERWIG 7.

4. Evolution of the sub-structure observables along the jet shower

For the study of jet shower evolution, we focus on measuring sub-structure observables at the first, second, and third splits along the harder branch by using the iterative SoftDrop technique [3]. It enables a study of self-similarity among the splits and also elucidates the effect of restricting available phase space for radiation due to virtuality evolution. z_g and R_g distributions at the first, second, and third splits are compared at varying jet kinematics ($p_{T,jet}$) or initiator kinematics ($p_{T,initiator}$). While comparing across the $p_{T,jet}$ provides a direct handle on the variation of initial jet momenta, comparing across the $p_{T,initiator}$ gives a direct handle on the splitting kinematics.

4.1. *2+1D unfolding*

As in the previous section, multi-dimensional unfolding needs to be implemented. z_g and R_g at a given split and given $p_{T,initiator}$ or $p_{T,jet}$ are unfolded via 2D Iterative Bayesian method described in Sec. 3.1. Splitting hierarchy is modified going from particle level to detector level, so additional correction is applied by matching the splits at particle level to detector level via requiring $\Delta R < 0.1$ between the prongs that initiate the splits. The 2D unfolded distributions are weighted based on the split matching and then summed appropriately, resulting in fully corrected z_g and R_g distributions at varying splits and jet or initiator momenta.

4.2. *Results and Monte Carlo comparisons*

Fully unfolded distributions for z_g and R_g at the first, second and third splits are shown in Fig. 4. Top panels show z_g distributions at first (black), second (red) and third (blue) splits for two different $p_{T,initiator}$ bins. Bottom panels show R_g distributions for two different $p_{T,jet}$ bins. Shaded bands around the data points correspond to the total systematic uncertainties, as described in Sec. 3.2, with the uncertainty due to prior shape variation included. We include an additional source of shape uncertainty due to the split matching criterion varied by ± 0.025.

We observe significant changes to both z_g and R_g as we move from the first to the third split. R_g distributions become narrower with increasing split numbers, and z_g distributions change from asymmetric splitting to a flatter distribution with more symmetric splits. Only a weak dependence on the $p_{T,\text{initiator}}$ or $p_{T,\text{jet}}$ is observed, which points to the split number being the driving factor.

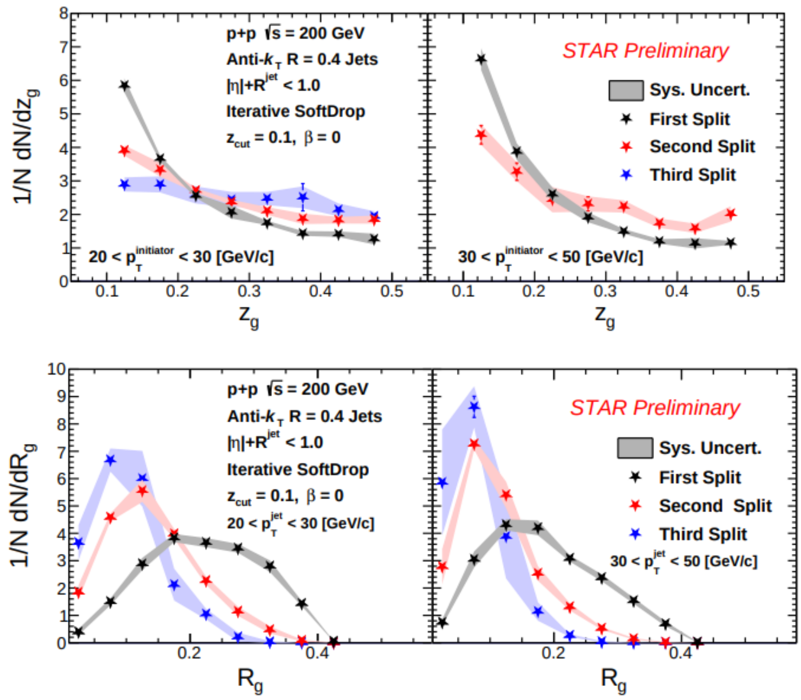

Fig. 4. Fully unfolded z_g (top) and R_g (bottom) distributions for different splits in p+p collisions at $\sqrt{s}$ = 200 GeV. The top (bottom) panels are differential in initiator (jet) p_T for two bins $20 < p_T < 30$ GeV/c (left) and $30 < p_T < 50$ GeV/c (right).

In Fig. 5 fully unfolded R_g distributions for the first, second, and third splits are compared with MC simulations, which are seen to describe the trend of the data.

4.3. *Conclusions*

We presented the first fully corrected distributions of z_g vs. R_g as a function of $p_{T,\text{jet}}$ at the first split, and z_g and R_g distributions as a function of $p_{T,\text{jet}}$ or $p_{T,\text{initiator}}$ for the first, second, and the third splits. We observe significant variation of the splitting kinematics as we select on emissions of small to large R_g. Similarly, we also note that selecting on the split number as we move along the jet shower mimics the same observation as selecting on R_g. These results imply an inherent correlation between the dynamics of splits and the available phase-space for radiation. We observe only a weak dependence of the splitting kinematics on $p_{T,\text{jet}}$ or $p_{T,\text{initiator}}$. We also compared data with the Monte

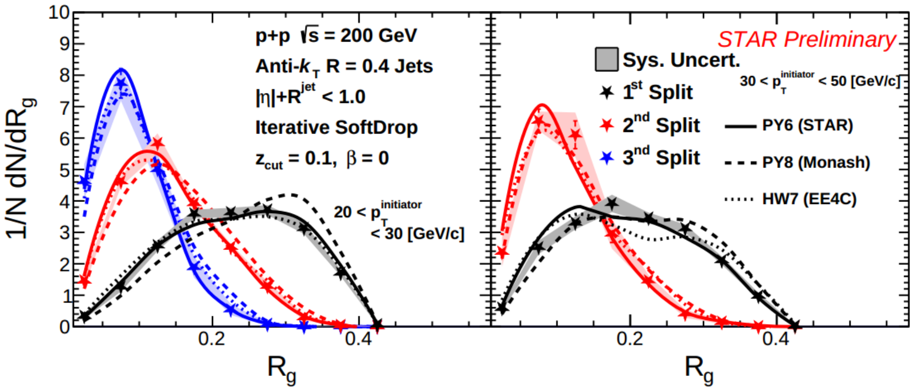

Fig. 5. Fully unfolded z_g and R_g distributions for different splits and various $p_{T,\text{initiator}}$ bins, $20 < p_T < 30$ GeV/c (left) and $30 < p_T < 50$ GeV/c (right), in p+p collisions at $\sqrt{s}$ = 200 GeV, compared with MC simulations from PYTHIA 6, PYTHIA 8 and HERWIG 7.

Carlo simulations, which qualitatively capture the trend of the data. In the upcoming publication, the data will be compared to models with varying implementations of perturbative (parton showers) and non-perturbative (hadronization/MPI/UE) models to understand the impact of each regime along the jet shower.

Acknowledgments

The work has been supported by the grant LTT18002 of Ministry of Education, Youth and Sports of the Czech Republic.

References

1. A. J. Larkoski, S. Marzani, G. Soyez and J. Thaler, *Journal of High Energy Physics* **2014** (2014), doi:10.1007/JHEP05(2014)146.
2. CMS Collaboration (doi:10.1007/JHEP05(2014)146) (7 2009).
3. F. A. Dreyer, L. Necib, G. Soyez and J. Thaler, *JHEP* **06**, 093 (2018), http://arxiv.org/abs/1804.03657`arXiv:1804.03657 [hep-ph]`, doi:10.1007/JHEP06(2018)093.
4. K.H. Ackermann et al., *Nuclear Instruments and Methods in Physics Research Section A: Accelerators, Spectrometers, Detectors and Associated Equipment* **499**, 624 (2003), doi: https://doi.org/10.1016/S0168-9002(02)01960-5.
5. J. Adam et al., *Physics Letters B* **811**, 135846 (2020), doi:https://doi.org/10.1016/j.physletb.2020.135846.
6. L. Havener, *Nuclear Physics A* **1005** (2021), doi:10.1016/j.nuclphysa.2020.121906.
7. G. Aad et al., *Physical Review Letters* **124**, 222002 (2020), doi:10.1103/PhysRevLett.124.222002.
8. A. M. Sirunyan, et al., *Physical Review Letters* **120** (2018), doi:10.1103/PhysRevLett.120.142302.

9. STAR Collaboration Collaboration (Abdallah, M. S. et al.), *Phys. Rev. D* **104**, 052007 (Sep 2021), doi:10.1103/PhysRevD.104.052007.
10. T. Sjöstrand, S. Mrenna and P. Skands, *Journal of High Energy Physics* **2006**, 026 (2006-05-01), doi:10.1088/1126-6708/2006/05/026.
11. P. Z. Skands, *Physical Review D* **82** (2010), doi:10.1103/PhysRevD.82.074018.
12. R. Brun, R. Hagelberg, M. Hansroul and J. C. Lassalle (7 1978).
13. T. S. et al., *Computer Physics Communications* **191**, 159 (2015), doi:10.1016/j.cpc.2015.01.024.
14. P. Skands, S. Carrazza and J. Rojo, *The European Physical Journal C* **74** (2014), doi: 10.1140/epjc/s10052-014-3024-y.
15. J. Bellm et al., *The European Physical Journal C* **76** (2016), doi:10.1140/epjc/s10052-016-4018-8.
16. M. Seymour and A. Siodmok, *Journal of High Energy Physics* **2013** (10 2013), doi: 10.1007/JHEP10(2013)113.